ON THE GEOMETRY OF THE X-RAY–EMITTING REGION IN SEYFERT GALAXIES

Boris E. Stern,[1,2] Juri Poutanen,[2] Roland Svensson,[2]
Marek Sikora,[2,3] and Mitchell C. Begelman[4,5]
Received 1995 February 13; accepted 1995 May 26

ABSTRACT

For the first time, detailed radiative transfer calculations of Comptonized X-ray and γ-ray radiation in a hot pair plasma above a cold accretion disk are performed using two independent codes and methods. The simulations include both energy and pair balance as well as reprocessing of the X- and γ-rays by the cold disk. We study both plane-parallel coronae as well as active dissipation regions having shapes of hemispheres and pill boxes located on the disk surface. It is shown, contrary to earlier claims, that plane-parallel coronae in pair balance have difficulties in self-consistently reproducing the *ranges* of 2–20 keV spectral slopes, high-energy cutoffs, and compactnesses inferred from observations of type 1 Seyfert galaxies. Instead, the observations are consistent with the X-rays coming from a number of individual active regions located on the surface of the disk.

A number of effects such as anisotropic Compton scattering, the reflection hump, feedback to the soft photon source by reprocessing, and an active region in pair equilibrium all conspire to produce the observed *ranges* of X-ray slopes, high-energy cutoffs, and compactnesses. The spread in spectral X-ray slopes can be caused by a spread in the properties of the active regions such as their compactnesses and their elevations above the disk surface. Simplified models invoking isotropic Comptonization in spherical clouds are no longer sufficient when interpreting the data.

Subject headings: accretion, accretion disks — galaxies: Seyfert — gamma rays: theory — radiation mechanisms: thermal — radiative transfer — X-rays: general

1. INTRODUCTION

X-ray spectra of Seyfert 1 galaxies in the 2–18 keV range show an intrinsic power-law component with intensity index in the range $\alpha = 0.9$–1.0 superimposed on a component arising from reflection (and reprocessing) of the intrinsic power law by cold opaque matter (e.g., the analysis of 60 spectra from 27 Seyfert galaxies by Nandra & Pounds 1994). The overall 2–18 keV spectral index is distributed around a mean value of $\alpha_{2-18} = 0.73$ with a dispersion of 0.15. The reprocessing matter must subtend $\sim$ 1–2 π solid angle as viewed from the X-ray source. Combined *Ginga* and *Compton Gamma Ray Observatory* (*CGRO*) OSSE observations show a spectral cutoff of the intrinsic power-law component in the several hundred keV range both for IC 4329A (Zdziarski et al. 1994; Madejski et al. 1995) and for the average spectrum of a sample of Seyfert 1's (Zdziarski et al. 1995). NGC 4151 differs in several respects, lacking a reflection component and having its cutoff at about 50 keV (Maisack et al. 1993; Zdziarski, Lightman, & Maciolek-Niedźwiecki 1993), and thus requires special considerations (Sikora et al. 1995). A strong annihilation line, predicted by nonthermal models (e.g., review by Svensson 1994), has never been detected. The strong UV bumps indicated in many sources require the existence of thermally radiating cold matter in the compact region where most of the power is released.

These data are broadly consistent with a geometry where the hot X-ray–emitting gas is located above the cold accretion disk (as proposed, e.g., by Paczyński 1978). Such a cold disk is one of the main features in the canonical black hole models of active galactic nuclei (AGNs). The data favor *thermal* Comptonization of the disk UV radiation as the main process by which hot electrons generate the power-law X-rays (Haardt & Maraschi 1991). About half the X-rays impinge on the cold disk and are reprocessed, emerging mostly as soft blackbody radiation, in addition to any blackbody radiation from internal dissipation in the disk. Haardt & Maraschi (1991) emphasized the coupling between the corona and the cold disk resulting from reprocessing, as the soft photons affect the cooling of the hot corona. In order for the Comptonized spectrum to have a power-law index close to unity, nearly all the power must be dissipated in the hot gas. Consequently, the soft blackbody UV luminosity, L_s, should be of about the same magnitude as the hard Comptonized X-ray luminosity, L_h, that leaves the corona-disk system. This is contrary to observations, which show that L_s is often several times larger than L_h. Another important consequence of the corona-disk geometry (in which the soft photons enter the corona from only one side) is that the source of soft photons is anisotropic. To deal with effects arising from anisotropy, which had been neglected in previous treatments, Haardt (1993) developed an approximate theory for anisotropic Compton scattering in a hot slab. Haardt & Maraschi (1993, hereafter HM93) then applied this theory to the corona-disk geometry, including reprocessing by the cold disk and imposing pair balance in the hot slab. The latter constraint is crucial, since the coronal temperatures and "compactnesses" are sufficiently high that pair production could account for most of the scattering medium. HM93 claim that the resulting X-ray spectral slopes and compactnesses are in excellent agreement with observations.

The pair balance calculations by HM93, however, suffer

[1] Institute for Nuclear Research, Russian Academy of Sciences, Moscow 117312, Russia; stern@inr.msk.su.

[2] Stockholm Observatory, S-133 36 Saltsjöbaden, Sweden; juri@astro.su.se, svensson@astro.su.se.

[3] Nicolaus Copernicus Astronomical Center, Bartycka 18, 00-716 Warsaw, Poland; sikora@camk.edu.pl

[4] JILA, University of Colorado, Boulder, CO 80309; mitch@jila .colorado.edu.

[5] Also at Department of Astrophysical, Planetary, and Atmospheric Sciences, University of Colorado, Boulder, CO 80309.

from adopting the *prescription* in Zdziarski (1985) for the Comptonized spectra including a simple exponential cutoff at photon energies above kT_e. Since the dimensionless coronal temperature, $\Theta \equiv kT_e/m_e c^2$, is less than unity in these simulations, only photons in the exponential tail can produce pairs. Self-consistent coronal temperatures, Θ, and Thomson scattering optical depths, τ_T, are obtained by first solving the Comptonization and energy balance problem in the hot gas. However, if the prescribed spectral shapes at pair-producing energies are erroneous, one will derive erroneous compactnesses when solving the pair balance equation for given (Θ, τ_T). This would then lead to incorrect conclusions regarding the spectral properties as a function of compactness for slab geometry.

In this paper, we use two different and independent methods of solving exactly the radiative transfer/Comptonization problem in mildly relativistic (or relativistic) thermal plasmas, taking into account energy and pair balance and cold disk reprocessing (including angular anisotropy and Klein-Nishina effects). For a given compactness in *slab geometry*, we find temperatures and spectral slopes which are *incompatible* both with HM93's approximate model and with observations. However, models with *localized active regions*, simulated by hemispheres or pillboxes atop a cold disk, can reproduce the observations easily. The latter type of geometry was recognized by Haardt, Maraschi, & Ghisellini (1994) as a way of avoiding the rough equality of L_s and L_h that is inevitable in uniform slab models.

The first method used in our calculations is based on the Nonlinear Monte Carlo (NLMC) method developed by Stern (1985, 1988) and described in detail in Stern et al. (1995). This method can follow particles and photons interacting with a background medium consisting of the same particles and photons (this is the nonlinearity) in both steady and time-dependent systems with any chosen geometry. In the present case, only photons are followed, while the electrons and positrons are assumed to be thermal. The second method is a pure one-dimensional radiative transfer code for Compton scattering in relativistic plasmas developed by Poutanen (1994; see also Poutanen & Vilhu 1993) using the iterative scattering method (ISM), where the radiative transfer equation is solved for each scattering order (e.g., Sunyaev & Titarchuk 1985; Haardt 1994). A thorough discussion of the latter ISM code and a comparison with results obtained using the NLMC code will appear in Poutanen et al. (1995).

In § 2 we apply these methods to coronal slabs, and in § 3 we apply them to two geometries for active regions, finding that the results for active regions are more consistent with observations.

2. COMPTONIZATION IN PLANE-PARALLEL PAIR CORONAE (SLABS)

2.1. *Setup*

In both types of simulations, a local dissipation compactness, $l_{diss} \equiv (L_{diss}/h)(\sigma_T/m_e c^3)$, characterizes the dissipation with L_{diss} being the power providing uniform heating in a cubic volume of size h in the slab, where h is the height of the slab. For the purpose of obtaining accurate radiative transfer, the slab is divided into 3–11 homogeneous spatial zones depending upon the expected τ_T. The reprocessed radiation has a flux equal to the absorbed incident flux and a Planckian spectral *shape*, but for simplicity the Planckian temperature T_{bb} is set to

a value of 5 eV, a typical blackbody temperature for canonical accretion disks in AGNs. We assume no internal dissipation in the cold disk. The two parameters, l_{diss} and T_{bb}, uniquely specify the slab simulations. We consider pure pair coronae, assuming that any coronal background plasma has a scattering optical depth much less than τ_T. For both types of codes, the system is relaxed toward a steady state as regards energy balance, pair balance, and emerging spectra. On a Sun IPX, a typical NLMC simulation takes a few hours, while the ISM code takes about 10 minutes for six angular gridpoints, seven spatial zones, and 80 frequency points.

2.2. *The Energy and Pair Balance in Slabs*

In the NLMC simulations, the spatial distributions of temperature and pair density are almost homogeneous, having a contrast of less than a factor of 2 between the top and bottom slab layers as a result of τ_T being less than unity. As output parameters, the temperature, T_e (or Θ), is averaged over height, and the vertical Thomson scattering optical depth, τ_T, is easily computed. With the ISM code, the energy balance and pair balance are solved using height-averaged Compton cooling and pair production, giving a typical temperature and pair density for the almost homogeneous slab. The *rectangles* and the *dashed curve* in Figure 1a show Θ versus l_{diss} obtained with the NLMC code and the ISM code, respectively. Figure 1b shows τ_T versus l_{diss} using the same notation. The agreement is very good.

Formally, the problem at hand can be solved in three steps. First, the radiative transfer/Comptonization problem together with energy conservation for the cold disk (i.e., reprocessed flux equals incident flux) is solved giving a relation between Θ and τ_T. As expected, the Θ versus τ_T relation obtained with the approximate treatment of HM93 agrees with our exact simulations to within a few percent up to our largest value of $\tau_T = 0.37$. The solutions are characterized by an almost constant generalized Kompaneets parameter, $y \equiv \tau_T(1 + \tau_T)$ $(4\Theta + 16\Theta^2)$. For the four NLMC solutions, $y \approx 0.48$, while for the ISM solutions, $y \approx 0.49$–0.53. Secondly, the energy balance of the corona is solved giving the *ratio* L_{diss}/L_s, or, alternatively, L_h/L_s (where typically $L_h \sim L_{diss}/2$). In the coronal energy balance, we account for the reduction of L_s which results from scattering of the reprocessed spectrum in the slab (important for $\tau_T \gtrsim 0.1$). For example, for $\tau_T = 0.37$ we find $L_h/L_s = 1.60$, while neglecting the effect (as in HM93) gives $L_h/L_s = 0.88$. Thirdly, the pair balance problem is solved for previously obtained combinations of Θ and τ_T, giving the absolute value of l_{diss} (= 10^3 for $\tau_T = 0.37$). We find that the corresponding values of l_{diss} obtained by HM93 (*dotted curve* in Fig. 1) are in error by up to a factor of 20 as a result of the spectrum prescribed by HM93 at photon energies, $h\nu > kT_e$.

2.3. *Spectra from Slabs*

For improved statistics with the NLMC method, the spectra are averaged over viewing angles $0.6 < \cos \theta < 1$, i.e., approximately the viewing angles expected for Seyfert 1 galaxies in the unified model. Here θ is the angle relative to the normal of the disk. With the ISM code, spectra are computed at the chosen angular gridpoints ($\cos \theta = 0.113$, 0.5, and 0.887) in the upward direction. The least square overall spectral slopes, α_{2-18}, for the 2–18 keV range were determined and are displayed in Figure 2 by the rectangles (using the NLMC code) and by the *dashed curve* (using the ISM code for $\cos \theta =$
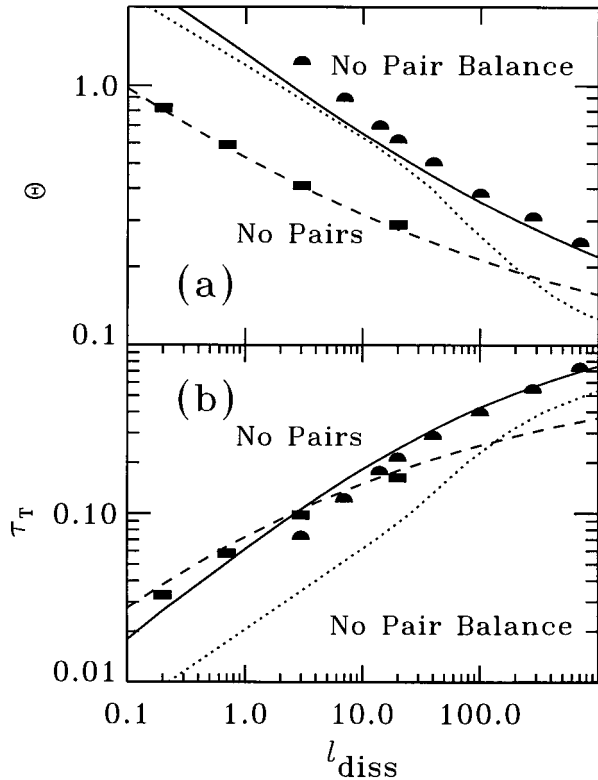
FIG. 1.—(*a*) Dimensionless temperature, $\Theta \equiv kT_e/m_ec^2$, vs. dissipation compactness, $l_{\text{diss}} \equiv (L_{\text{diss}}/h)(\sigma_T/m_ec^3)$, for a steady X-ray–emitting region in pair and energy balance located on a cold disk surface. The soft photons from the cold disk are assumed to have $kT_{\text{bb}} = 5$ eV. *Rectangles* and *dashed curve*: results from NLMC code and ISM code, respectively, for the case of a plane-parallel slab corona. *Dotted curve*: results for slabs from the approximate treatment of HM93. Results for individual active pair regions located on the disk surface are shown by *hemispheres* (hemisphere geometry using NLMC code) and *solid curve* (pillbox geometry using ISM code). The parameter space to the right of the respective curves is forbidden because pair balance cannot be achieved, and the parameter space to the left would contain solutions where the background coronal plasma dominates over the pairs, i.e., "pair-free" solutions (e.g., Svensson 1984; HM93). (*b*) Vertical Thomson scattering optical depth, τ_{T}, vs. dissipation compactness, l_{diss}. Same notation and parameters as in (*a*).
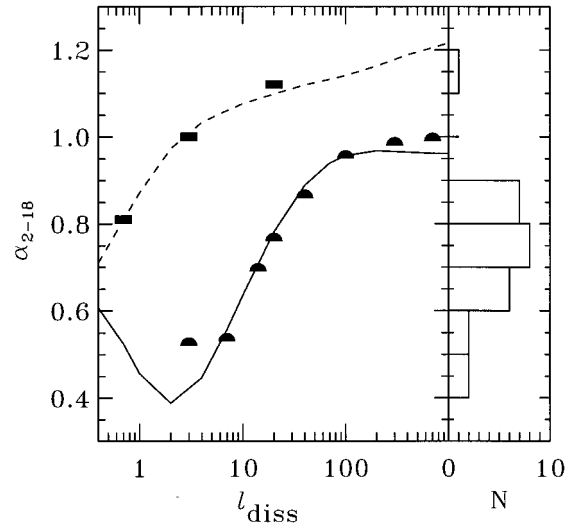

FIG. 2.—Overall spectral intensity index, α_{2-18}, least-square fitted to the model spectra in the 2–18 keV range vs. the dissipation compactness, l_{diss}. Same notation as in Fig. 1. The spectra from NLMC code were averaged over viewing angles $0.6 < \cos \theta < 1.0$ before determining α_{2-18}. For the ISM code, face-on spectra (at $\cos \theta = 0.887$) were used. The right panel shows the observed distribution of α_{2-18} for *Ginga* spectra from 27 Seyfert galaxies (Nandra & Pounds 1994).

0.887). For $l_{\text{diss}} > 1$ we find that α_{2-18} at $\cos \theta \sim 0.9$ (i.e., almost face on) and 0.5 differ by less than 5%, allowing comparisons between the face-on results using the ISM code and the average spectra from the NLMC code. The two codes give spectra that are in very good agreement, providing the first serious test of both codes. The right panel of Figure 2 shows the observed distribution of α_{2-18} for *Ginga* spectra from 27 Seyfert galaxies (Nandra & Pounds 1994). We conclude from Figure 2 that slabs must have $l_{\text{diss}} < 1$ in order to reproduce the observed range of α_{2-18}, which is in conflict with the best available (albeit uncertain) observed compactnesses ($l_h \sim l_{\text{diss}}/2 \sim 1$–100, e.g., Done & Fabian 1989).

We find our calculated spectra to be in qualitative, but not quantitative, agreement with the spectra in Figures 4*a*–4*c* in HM93. The true spectral shape at $h\nu > kT_e$ in an optically thin plasma has a slow cutoff, reflecting the thermal Compton scattering kernel [approximately $\propto \exp(-h\nu/2kT_e)$] rather than the more rapid ad hoc exponential cutoff, $\nu^{1-\alpha} \exp(-h\nu/kT_e)$, of HM93. Having too few pair-producing photons, HM93 obtained l_{diss} (they used notation l_c) up to a factor of 20 too large when solving the pair balance equation. Therefore,

HM93 erroneously found slab models to be in agreement with observed spectra and compactnesses.

3. COMPTONIZATION IN ACTIVE PAIR REGIONS

3.1. *Setup*

We represent the active regions in different ways with the two codes. With the NLMC code that fully handles two- and three-dimensional radiative transfer, we consider hemispheres of radius h located on the disk surface and divide them into five homogeneous spatial zones as shown in Figure 7 in Stern et al. (1995). The hemisphere problem is axisymmetric and thus two-dimensional. Since the ISM code can only handle one-dimensional problems, cylinders of pillbox shape of height h and diameter $2h$ were considered. By allowing reprocessed and reflected radiation to enter only at the bottom of the pillbox, assuming a nonzero source function only within the pillbox and averaging the computed radiation field over each spatial layer for each scattering order, we effectively convert the problem to a one-dimensional one. We also take account of the fact that not all the reprocessed X-ray radiation reenters the active region (about 60% for the hemisphere [see also Haardt 1994], about 50% for the pillbox). As for the slab case, these simulations depend on two parameters, l_{diss} and T_{bb}, but now L_{diss} is the power dissipated uniformly in the active region. As before, $T_{\text{bb}} = 5$ eV.

3.2. *The Energy and Pair Balance in Active Pair Regions*

In the output of our NLMC simulations, the computed temperature, T_e (or Θ), is averaged over volume, and a mean Thomson scattering optical depth, τ_{T}, is obtained by averaging over all radial directions of the hemisphere. With the ISM code, volume-averaged energy balance and pair balance are solved for a typical Θ and the vertical τ_{T} of the almost homogeneous pillbox. The *hemispheres* and *solid curves* in Figure 1*a* show Θ versus l_{diss} obtained with the NLMC code and the ISM code, respectively. Figure 1*b* shows τ_{T} versus l_{diss}
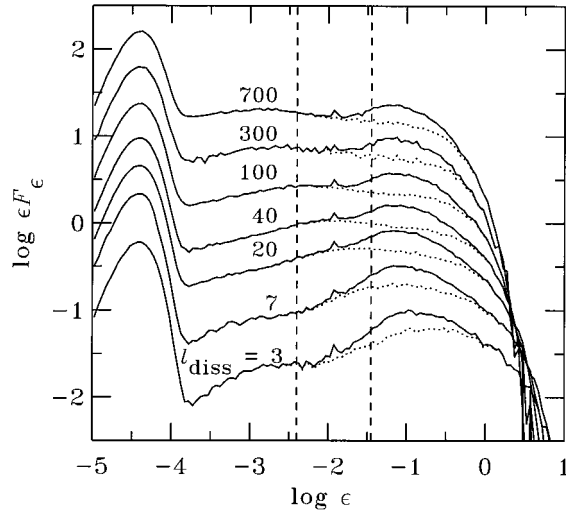
FIG. 3.—Emerging spectra, $\varepsilon F_\varepsilon$, where F_ε is the energy flux (arbitrary units) and $\varepsilon \equiv h\nu/m_e c^2$ from hemispheres of different compactnesses, $l_{\rm diss}$. The spectra are averaged over viewing angles $0.6 < \cos\theta < 1$. *Solid curves*: total spectrum which is the sum of the Comptonized spectrum from the hemisphere itself (*dotted curves*), the reprocessed blackbody spectrum, and the reflection component. *Dashed lines*: the 2–18 keV spectral range.

using the same notation. The parameter combinations $(\tau_{\rm T}, \Theta)$ obtained for different $l_{\rm diss}$ give an almost constant Kompaneets parameter, y. We find $y \approx 1.9$–2.2 for hemispheres and $y \approx 2.0$–2.4 for pillboxes. The reason for the larger y for active regions, as compared to slabs, is that fewer of the soft reprocessed photons return to the active region (yielding increased "photon starvation," e.g., Zdziarski, Coppi, & Lamb 1990), thus requiring harder spectra to achieve the needed Compton cooling, and correspondingly larger values of y.

At given $l_{\rm diss}$, values of Θ are larger for active pair regions as compared to pair slabs, while $\tau_{\rm T}$ is smaller at small $l_{\rm diss}$ and larger at large $l_{\rm diss}$. The closer the active pair regions are, the more they will influence each other by providing X-ray photons for Comptonization and >511 keV photons for pair production. Such "interacting" pair regions will have Θ and $\tau_{\rm T}$ in between the curves for slabs and active regions in Figure 1a. A slab corona is the limit of closely packed active regions. Active pair regions near disks have properties placing them in the parameter space in Figure 1a forbidden for pair slabs.

3.3. *Spectra from Active Pair Regions*

Figure 3 shows emerging spectra from hemispheres at different $l_{\rm diss}$. Each *solid curve* shows a total spectrum, being the sum of the Comptonized spectrum from the hemisphere (*dotted curve*), the reprocessed blackbody spectrum at 5 eV, and the reflection component. In mildly relativistic plasmas, Compton scattering in the forward direction is suppressed, causing the contribution of once scattered photons in face-on directions to be suppressed (HM93). This effect of anisotropy causes the Comptonized spectra (*dotted curves*) to be broken power laws with the *anisotropy break* occurring just above the peak energy of twice scattered photons. The power-law slope at energies above the break is related to the Kompaneets parameter, y. The fact that y is almost independent of $l_{\rm diss}$ shows through the almost constant spectral slope of the Comptonized spectra above the break. As $l_{\rm diss}$ increases and Θ

decreases, the break moves to lower energies through the 2–18 keV range, causing $\alpha_{2\text{-}18}$ to soften from 0.55 to 1. For viewing angles relevant to Seyfert 1 galaxies, the suppression of once-scattered photons does not affect the spectra in the 2–18 keV range except at small $l_{\rm diss}$, when this Compton order extends into that spectral range (see Fig. 3 for the case in which $l_{\rm diss} = 3$). The angle-averaging procedure we use washes out some of the anisotropy at lower energies but produces the correct $\alpha_{2\text{-}18}$, since there is little spread in $\alpha_{2\text{-}18}$ for the considered range of viewing angles.

The spectral slopes, $\alpha_{2\text{-}18}$, are shown in Figure 2 for both *hemispheres* and *pillboxes* (*solid curve*) as a function of $l_{\rm diss}$. The right panel shows the observed distribution of $\alpha_{2\text{-}18}$ for *Ginga* spectra from 27 Seyfert galaxies (Nandra & Pounds 1994). Active regions produce spectra covering the *observed ranges* of $\alpha_{2\text{-}18}$ (≈ 0.4–0.9) and cutoff energies ($\sim 2kT_e$) for the *observed range* of compactnesses ($l_h \sim l_{\rm diss}/2 \sim 1$–100; Done & Fabian 1989). The observed mean $\alpha_{2\text{-}18} \sim 0.7$ implies a preferred value of $l_{\rm diss} \sim 20$. Elevating the active region from the disk would make even fewer soft reprocessed photons return to the active region, requiring larger y and thus harder spectra. The corresponding *solid* curve would thus be lowered in Figure 2 by an amount depending upon the elevation. The observed dispersion of $\alpha_{2\text{-}18}$ could be caused by both a spread in $l_{\rm diss}$ and the elevation of active regions above the disk.

4. SUMMARY

Our results can be summarized as follows: (1) We have performed the first exact radiative transfer simulations of Comptonization by hot gas at mildly relativistic temperatures located in the vicinity of a cold disk, fully accounting for geometric effects, reprocessing, and self-regulation of the soft photon flux, pair, and energy balance. We have used two codes which rely on quite different methods and have obtained excellent agreement for cases where detailed comparison can be made. (2) We find that pair slab models with $T_{\rm bb} = 5$ eV have difficulties in reproducing the observed characteristics of type 1 Seyfert X-ray spectra, while active pair regions with geometries of, e.g., hemispheres or pillboxes produce X-ray spectra in much better agreement with observations. Whether this is still true for larger $T_{\rm bb}$ values remains to be seen. The dispersion of observed spectral behavior is likely a result of the active regions having a (nonuniform) spread in compactness and elevation above the disk. (3) Our findings support the idea of a structured or patchy corona with a number of separated active regions (e.g., flares and coronal loops) first suggested by Galeev, Rosner, & Vaiana (1979), and recently rejuvenated by Haardt, Maraschi, & Ghisellini (1994), who argued that active regions typically would have $l_{\rm diss} \sim 30$ in agreement with our preferred $l_{\rm diss}$. (4) Finally we conclude that simplified models neglecting effects of anisotropy and other geometric effects, reprocessing, and correct spectral behavior at pair-producing energies are no longer adequate when interpreting spectra.

REFERENCES

Done, C., & Fabian, A. C. 1989, MNRAS, 240, 81
Galeev, A. A., Rosner, R., & Vaiana, G. S. 1979, ApJ, 229, 318
Haardt, F. 1993, ApJ, 413, 680
———. 1994, Ph.D. thesis, SISSA, Trieste
Haardt, F., & Maraschi, L. 1991, ApJ, 380, L51
———. 1993, ApJ, 413, 507 (HM93)
Haardt, F., Maraschi, L., & Ghisellini, G. 1994, ApJ, 432, L95
Madejski, G. M., et al. 1995, ApJ, 438, 672
Maisack, M., et al. 1993, ApJ, 407, L61
Nandra, K., & Pounds, K. A. 1994, MNRAS, 268, 405
Paczyński, B. 1978, Acta Astron., 28, 241
Poutanen, J. 1994, Ph.D. thesis, Univ. Helsinki
Poutanen, J., et al. 1995, in preparation
Poutanen, J., & Vilhu, O. 1993, A&A, 275, 337
Sikora, M., et al. 1995, in preparation
Stern, B. E. 1985, Soviet Astron., 29, 306
———. 1988, Nordita/88-51 A, preprint
Stern, B. E., Begelman, M. C., Sikora, M., & Svensson, R. 1995, MNRAS, 272, 291
Sunyaev, R. A., & Titarchuk, L. G. 1985, A&A, 143, 374
Svensson, R. 1984, MNRAS, 209, 175
———. 1994, ApJS, 92, 585
Zdziarski, A. A. 1985, ApJ, 289, 514
Zdziarski, A. A., et al. 1994, MNRAS, 269, L55
———. 1995, ApJ, 438, L63
Zdziarski, A. A., Coppi, P. S., & Lamb, D. Q. 1990, ApJ, 357, 149.
Zdziarski, A. A., Lightman, A. P., & Maciolek-Niedźwiecki, A. 1993, ApJ, 414, L93